Identification of tetracycline combinations as EphB1 tyrosine kinase inhibitors for treatment of neuropathic pain

Mahmoud S. Ahmed[a,1], Ping Wang[a,1], Ngoc Uyen Nhi Nguyen[a], Yuji Nakada[a], Ivan Menendez-Montes[a], Muhammad Ismail[b], Robert Bachoo[a], Mark Henkemeyer[c], Hesham A. Sadek[a,d,e,f,2], and Enas S. Kandil[g,2]

[a]Department of Internal Medicine, University of Texas Southwestern Medical Center, Dallas, TX 75390; [b]Department of Pharmaceutical Chemistry, The British University in Egypt, Cairo 11837, Egypt; [c]Department of Neuroscience, University of Texas Southwestern Medical Center, Dallas, TX 75390; [d]Department of Molecular Biology, University of Texas Southwestern Medical Center, Dallas, TX 75390; [e]Department of Biophysics, University of Texas Southwestern Medical Center, Dallas, TX 75390; [f]Center for Regenerative Science and Medicine, University of Texas Southwestern Medical Center, Dallas, TX 75390; and [g]Department of Anesthesiology, University of Texas Southwestern Medical Center, Dallas, TX 75390

Edited by Robert J. Lefkowitz, HHMI, Durham, NC, and approved December 29, 2020 (received for review July 31, 2020)

Previous studies have demonstrated that the synaptic EphB1 receptor tyrosine kinase is a major mediator of neuropathic pain, suggesting that targeting the activity of this receptor might be a viable therapeutic option. Therefore, we set out to determine if any FDA-approved drugs can act as inhibitors of the EphB1 intracellular catalytic domain. An in silico screen was first used to identify a number of tetracycline antibiotics which demonstrated potential docking to the ATP-binding catalytic domain of EphB1. Kinase assays showed that demeclocycline, chlortetracycline, and minocycline inhibit EphB1 kinase activity at low micromolar concentrations. In addition, we cocrystallized chlortetracycline and EphB1 receptor, which confirmed its binding to the ATP-binding domain. Finally, in vivo administration of the three-tetracycline combination inhibited the phosphorylation of EphB1 in the brain, spinal cord, and dorsal root ganglion (DRG) and effectively blocked neuropathic pain in mice. These results indicate that demeclocycline, chlortetracycline, and minocycline can be repurposed for treatment of neuropathic pain and potentially for other indications that would benefit from inhibition of EphB1 receptor kinase activity.

EphB receptor | drug repurposing | neuropathic pain | crystallography

Chronic pain is a common debilitating condition which typically results in prescriptions of high doses of opioids in an attempt to control the pain severity (1). In the United States, over 100 million patients are affected by a form of chronic pain, which results in significant morbidity and costs over $600 billion in combined lost wages and medical expenses annually. In fact, it is estimated that over 25 million Americans experience pain on a daily basis (2). Due to these staggering numbers and its link to opioid use, chronic pain has been dubbed "the silent epidemic" by the NIH (3). As a result of this chronic pain epidemic, the use of opioids has increased exponentially in the United States since the late 1990s (4) and has reached the level of a national crisis.

Although opioids are commonly used for treatment of chronic pain, they are only partially efficacious for short-term pain management, and the response to their long-term use is widely variable (5). Despite the magnitude of the pain epidemic and the opioid crisis, there has been little progress in the development of nonopioid alternative therapies. Therefore, there is an urgent need for developing novel nonopioid and nonaddicting therapies that are effective in management of chronic pain, as well as counteracting the adverse, highly addictive effects of opioid use, in particular opioid dependence and opioid withdrawal-mediated pain (6). Importantly, the path to new drug development is lengthy and costly. For example, it takes an average of 12 y and over $2 billion for a new drug to reach the market. These staggering statistics underscore the importance of developing faster and cheaper strategies to counteract the growing opioid epidemic.

Peripheral neuropathic pain (PNP), which is defined by neuralgia and painful polyneuropathy, is a highly prevalent type of pain that results in significant morbidity and disability (7–9). PNP is one of the common associated manifestations for a series of different diseases, such as autoimmune diseases, diabetes, different types of cancers, neurofibromatosis, viral infections, and toxin exposure, among others (10–16). Current therapies for treatment of PNP include over-the-counter drugs such as ibuprofen and acetaminophen, in addition to prescription pain medication including opioids, anticonvulsants, and antidepressants (17, 18). However, these therapies are seldom effective, in particular opioids, which, as outlined above, are ineffective for treatment of chronic pain, requiring dose escalation which further contributes to the ongoing opioid crisis.

The large family of Eph (erythropoietin-producing hepatocellular carcinoma) receptor tyrosine kinases have been implicated in numerous pathologies, including Alzheimer's disease, anxiety, neuropathic pain, malignancies, fibrotic diseases, and viral infections, among others (19–22). Eph receptors are highly conserved proteins that are divided into two subfamilies of nine EphA and five EphB receptors based on sequence similarity (23). As both Eph receptors and ephrins are membrane anchored,

Significance

Chronic pain is one of the most pressing national healthcare problems, and as a result, chronic pain was named by the NIH as the "silent epidemic." Consequentially, chronic pain has directly contributed to the disproportionate increase in opioid use in America. However, thus far, there has been little progress in discovery of alternative noninvasive therapeutics for chronic pain. The current report outlines the repurposing of three tetracyclines for treatment of neuropathic pain by targeting the catalytic domain of EphB1 kinase. These results can be readily applicable clinically for treatment of neuropathic pain and provide proof of concept for the development of molecules for targeting Eph/ephrin-mediated pathologies.

Author contributions: H.A.S. and E.S.K. designed research; M.S.A., P.W., N.U.N.N., Y.N., I.M.-M., M.I., R.B., M.H., and E.S.K. performed research; M.S.A., P.W., N.U.N.N., Y.N., I.M.-M., R.B., M.H., and H.A.S. analyzed data; and H.A.S. and E.S.K. wrote the paper.

The authors declare no competing interest.

This article is a PNAS Direct Submission.

[1]M.S.A. and P.W. contributed equally to this work.

[2]To whom correspondence may be addressed. Email: hesham.sadek@utsouthwestern.edu or enas.kandil@utsouthwestern.edu.

This article contains supporting information online at https://www.pnas.org/lookup/suppl/doi:10.1073/pnas.2016265118/-/DCSupplemental.

Published February 24, 2021.

receptor–ligand interactions generally occur upon cell–cell contact, and this leads to the transduction of bidirectional intracellular signals into both the Eph-expressing cell and ephrin-expressing cell.

Previous studies using *EphB1*$^{-/-}$ knockout mice and other approaches demonstrated that the EphB1 receptor tyrosine kinase protein is essential for neuropathic pain induced by different types of experimental nerve damage and for the related painful effects of opioid withdrawal (24–28). These studies also demonstrated that the EphB1 receptor mediates neuropathic pain directly in the spinal cord through activation of the n-methyl-d-aspartate receptor (NMDAR) which results in immediate early gene expression (c-Fos) and long-term potentiation, which are well documented to participate in chronic pain states and opioid withdrawal via the mechanism of central sensitization in the spinal cord. A key feature is that, following peripheral nerve damage, presynaptic ephrin-B2 ligand protein is up-regulated in nociceptive peripheral nerve fibers, and postsynaptic EphB1 receptor protein becomes up-regulated on dorsal horn neurons in the spinal cord. This model of ephrin-B2 and EphB1 in neuropathic pain and the ephrin-B:EphB:NMDAR protein interactions has been validated by numerous groups (29–43). Furthermore, what makes the EphB1 receptor a highly significant and important therapeutic target for neuropathic pain is that the knockout mouse shows no major developmental abnormalities and exhibits normal perception of acute/normal pain stimuli. Intriguingly, even the *EphB1*$^{+/-}$ heterozygote animals are refractory to neuropathic pain. This indicates reducing EphB1 activity 50% will likely be sufficient to mount a positive response. We therefore postulated that inhibitory compounds do not need to completely block EphB1 activity; they only need to reduce it. Therefore, we performed in silico analysis of Food and Drug Administration (FDA)–approved drugs for inhibitors of the EphB1 kinase domain. These studies allowed us to identify a group of tetracycline antibiotics as candidate FDA-approved drugs to be repurposed for treatment of neuropathic pain.

Despite their high relevance to a wide range of diseases, there are currently no approved FDA drugs targeting any of the Eph receptors. Conceptually speaking, drug repositioning can be a plausible approach toward screening of FDA-approved drugs with well-documented safety profiles and therapeutic indices to identify any with the potential to target Eph receptors. Herein, we present a drug-repositioning platform coupled with in vitro and in vivo evaluation for FDA-approved drugs that inhibit EphB receptors. Taking advantage of in silico screening, molecular biology, structural biology, biochemistry, and in vivo mouse models, we identify members of the tetracycline family including chlortetracycline, demeclocycline, and minocycline, used as antibiotics to treat a wide variety of bacterial infections (44), as potential drugs to repurpose for the treatment of PNP.

Results

In Silico Screen for EphB Kinase Inhibitors. The EphB receptors have highly conserved intracellular tyrosine kinase catalytic domain (45, 46). Crystal structures for EphB kinase domains have been determined and can be accessed in the protein data bank (PDB), such as 3ZFX (apo EphB1) and 5MJA (EphB1 bound with quinazoline-based inhibitor), 3ZFM (apo EphB2), 3ZFY (apo EphB3), and 3ZEW (EphB4 bound with staurosporine) (47, 48). We have coupled two different approaches related to drug discovery via employment of ligand-based and structure-based in silico screening, starting with staurosporine, which is bound with EphB4. Staurosporine was selected as a starting query for a ligand-based approach because of its broad ability to bind within many different kinase domains and the possessing of different functional moieties that will allow including all the potential hits (Fig. 1*A*). The MMFF94 energy-minimized library of FDA-approved drugs was screened for molecular similarity compared to staurosporine. The top 100 drugs based on Tanimoto chemical similarity score were further filtered based on literature survey and exclusion of drugs with undesirable clinical indications/side effects. This was followed by an in silico docking study along with the pocket of EphB1 kinase domain for ATP and/or inhibitor binding (PDB code: 5MJA) ending up with top 10 drugs (Fig. 1 *B* and *C* and *SI Appendix*, Table S1). Demeclocycline, chlortetracycline, rolitetracycline, oxytetracycline, ertapenem, darifenacin, quinagolide, minocycline, ramelteon, and galantamine showed proper binding affinity with respect to energy scoring (49), Tanimoto scores (50), and binding mode toward EphB1 kinase domain, suggesting hydrophobic–hydrophobic and a network of hydrogen bond interactions (Fig. 1 *D* and *E* and *SI Appendix*, Fig. S1).

Biochemical Evaluation of EphB Kinase Inhibitors. Seven of the identified FDA-approved drugs were first tested for their inhibitory profiles using an in vitro EphB1 kinase assay. Ramelteon, oxytetracycline, galantamine, and darifenacin failed to inhibit the EphB1 kinase activity at concentrations up to 100 μM (*SI Appendix*, Fig. S2). However, chlortetracycline, demeclocycline, and minocycline inhibited the EphB1 kinase activity with inhibition concentration at 50% (IC_{50}) calculated to be 39, 44, and 56 μM, respectively (Fig. 2). The ability of demeclocycline, chlortetracycline, and minocycline to inhibit EphB1 kinase activity prompted us to determine if they are also able to inhibit the related EphB2, EphB3, and EphB4 kinase domains, revealing all could be inhibited with IC_{50} ranging from 37 to 92 μM (Fig. 2). Curiously, chlortetracycline, demeclocycline, and minocycline all showed a similar biphasic influence on the EphB3 catalytic activity, in the low nanomolar ranges they slightly elevated activity, whereas at higher concentrations, they inhibited activity. Such biphasic responses were not observed with the EphB1, EphB2, and EphB4 kinase domains.

We determined the IC_{50} against EphB kinases for two-drug and three-drug combinations for the demeclocycline (D), chlortetracycline (C), and minocycline (M) to minimize the therapeutic dose per drug by having equimolar ratios of DC (demeclocycline + chlortetracycline), DM (demeclocycline + minocycline), and MC (minocycline + chlortetracycline) which demonstrated improvement in the IC_{50} against EphB1 at 16, 13, and 15 μM, respectively (*SI Appendix*, Fig. S3), compared to the staurosporine inhibitory profile (*SI Appendix*, Fig. S4). Exploring the triple-drug strategy by having equimolar ratio of MCD (minocycline + chlortetracycline + demeclocycline) improved the IC_{50} towards EphB1 kinase to 8 μM. Furthermore, we performed a kinase screen on 88 tyrosine kinase and tyrosine kinase-like kinases for MCD to determine its selectivity. The results indicate that only FGF-R1 had a residual activity of <50% (34%) following treatment with 40-μM MCD (*SI Appendix*, Table S2).

Structure Basis for EphB1 Inhibition. To investigate the structural basis of the three tetracyclines in EphB1 inhibition, we determined the crystal structure of apo EphB1 (PDB code: 7KPL) at 2.7 Å and the EphB1 kinase domain in complex with chlortetracycline (PDB code: 6UMW) at 1.98 Å by soaking the crystals in the solution containing the compound (*SI Appendix*, Fig. S3 and Table S3). EphB1 in complex with its byproduct adenosine diphosphate (ADP) (PDB code: 7KPM) at 1.6 Å was also determined to provide insights into the cofactor binding profile in the catalytic pocket. The overall structure of EphB1 bound with chlortetracycline adopts the traditional bilobed kinase fold similar to apo EphB1 and the structure of EphB1 bound with ADP with a core RMSD of 0.13 Å for 243 C-α atoms and 0.13 Å for 215 C-α atoms, respectively (Fig. 3*A*). The structure demonstrates that chlortetracycline lies in the catalytic pocket where ADP binds (Fig. 3*A*). For the chlortetracycline-bound structure, clear electron density for chlortetracycline is visible near the catalytic pocket (Fig. 3 *B* and *C* and *SI Appendix*, Fig. S6), which is similar to the ADP binding pocket and the quinazoline-based inhibitor-binding pocket. Chlortetracycline is stabilized in the catalytic pocket by

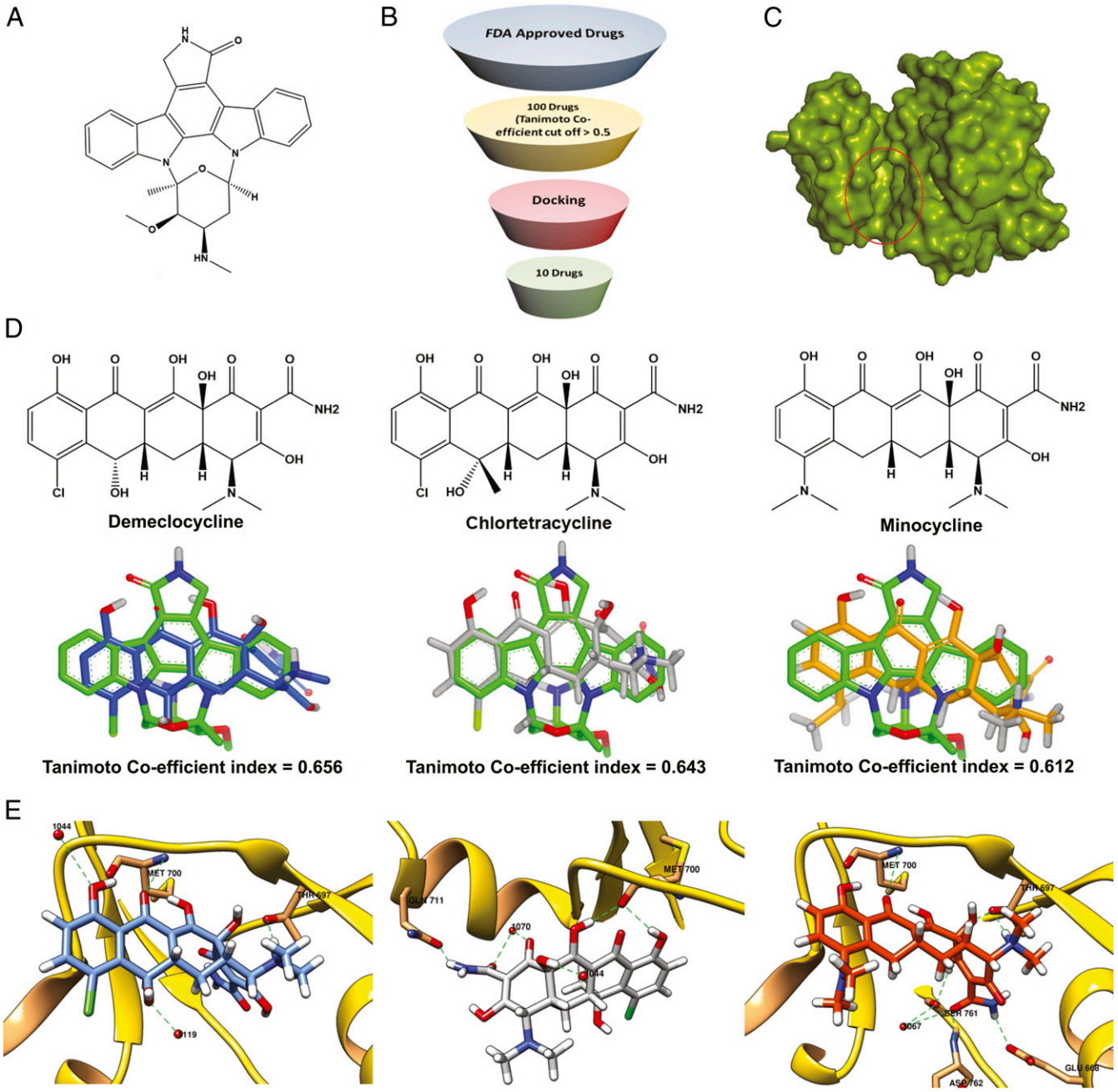

Fig. 1. In silico molecular modeling simulations. (*A*) Staurosporine structure was selected as query for molecular similarity simulations. (*B*) A schematic flowchart for the in silico molecular virtual screening, starting with energy minimized FDA-approved small molecules using MMFF94 force field to be checked for degree of superimposition based on Staurosporine. This was followed by selecting the top 100 hits based on their Tanimoto coefficient ratio to undergo a semiflexible docking study using MOE to end up with the top 10 drug candidates. (*C*) A Space-filling representation for EphB1 tyrosine kinase domain, where the red circle refer to the binding domain of identified small molecules. (*D*) The 2D chemical structures of demeclocycline (blue), chlortetracycline (gray), and minocycline (orange) and their structural superimposition, along with Staurosporine (green). (*E*) A visual representation of demeclocycline docked with EphB1 Kinase domain, showing hydrophobic interaction, and dotted green lines represent hydrogen bonding along with Met-700:A and Thr-697:A; chlortetracycline (gray), where hydrogen bonds situated along with MET 700:A and GLN 711:A, and minocycline (orange), where hydrogen bonds along with MET 700:A and GLU 668:A.

numerous favorable interactions (Fig. 3*C*). The first three aromatic rings are sandwiched by I625, V633, F699, and L751, and there are several hydrogen bond interactions with the side chain of T697 and the main chain of E698 and M700, which is also consistent with our prediction (Fig. 3*C* and *SI Appendix*, Fig. S5). In addition, the key interacting residues with chlortetracycline including T697, E698, and M700 are also critical for the interaction with ADP, which further validates that chlortetracycline functions as an ATP competitor in the catalytic pocket of EphB1 (*SI Appendix*, Fig. S6).

In Vivo Biological Evaluation. Peripheral tissue inflammation can cause the initiation and progression of acute and chronic pain with numerous manifestations of neuropathic pain, mediated by mechanisms including thermal hyperalgesia and mechanical allodynia (51, 52). We conducted validation experiments to evaluate

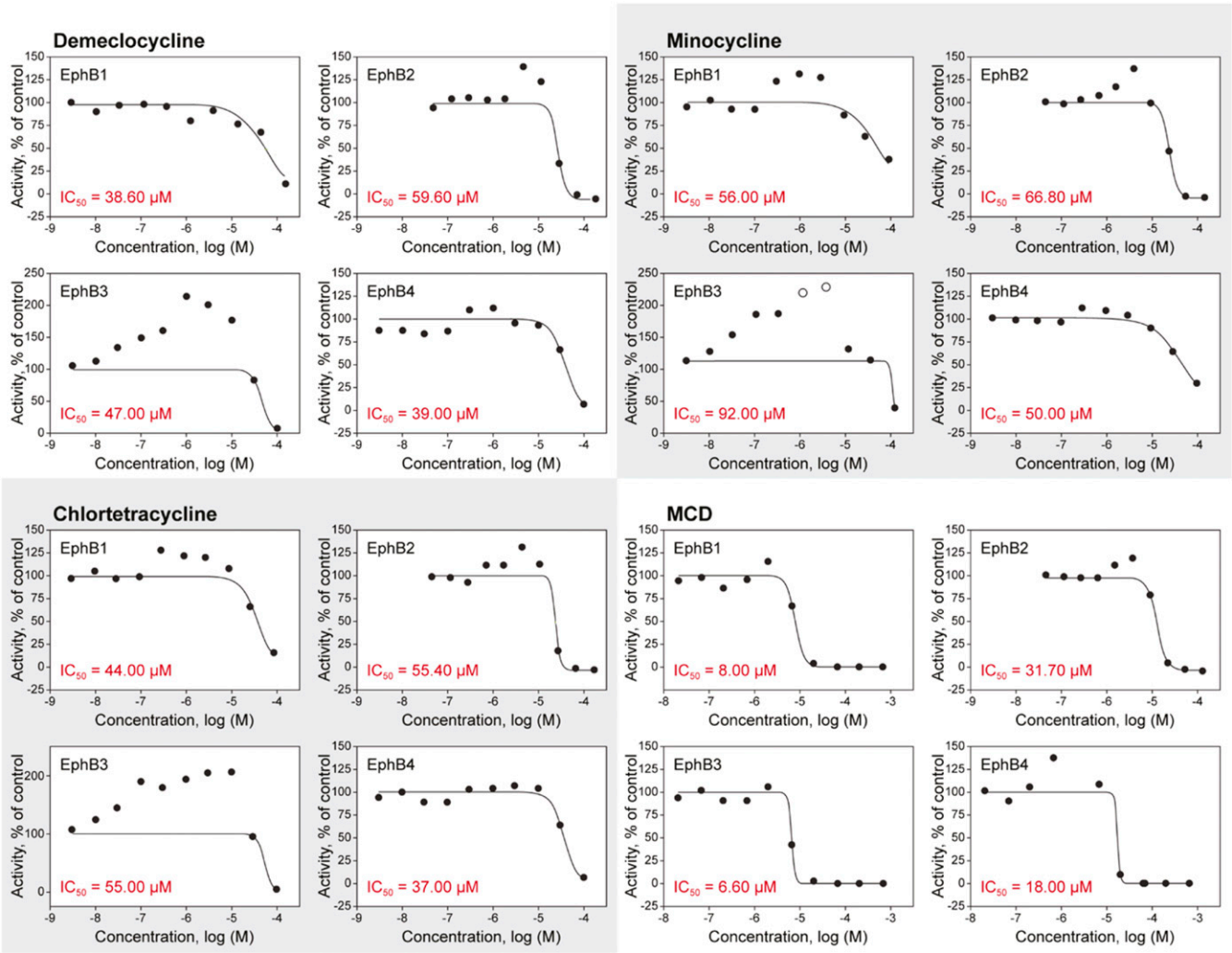

Fig. 2. Evaluation of demeclocycline, minocycline, and chlortetracycline, and MCD as EphB kinase inhibitors. The dose–response curves show the Inhibitory Concentration at 50% (IC_{50}) curves of demeclocycline, chlortetracycline, minocycline, and MCD (an equimolar ratio of minocycline, chlortetracycline, and demeclocycline) inEphB1, EphB2, EphB3, and EphB4 protein kinase activity assays. A radiometric in vitro protein kinase assay (33PanQinase Activity Assay) was used, where different concentrations of the drugs ranging from 1×10^{-4} M to 3×10^{-9} M were tested for their inhibitory activity in four different kinase domains. IC_{50} values were calculated based on the residual activity (percent) for the ability of the drugs to inhibit four protein kinases; open circles: activity values excluded to allow for the calculation of an IC_{50} value.

the in vivo effect of demeclocycline, DC, and MCD to reverse thermal hyperalgesia and mechanical allodynia stimuli.

In Vivo Evaluation Using Capsaicin-Induced Pain Model. Initially, we used capsaicin as a model for short neuropathic pain stimulus and tested two stimuli, thermal hyperalgesia using Hargreaves test and mechanical allodynia using von Frey test. The drugs were administered via gavage three consecutive days before capsaicin injection in the right hind paw, while the left hind paw remained uninjected as a control, where the whole experiment was conducted within 1 to 2 h before the clearance of the capsaicin effect. Demeclocycline [20 mg/kg/day, p.o (per os)], DC (7 mg/kg/day, p.o), and MCD (5 mg/kg/day, p.o) prolonged the paw withdrawal latency of the injected paw significantly compared to the controls (phosphate buffer saline [PBS] treated mice) upon exposure to thermal stimulus. The same behavior was observed upon exposure to mechanical stimulus with the three tested formulas (Fig. 4*A*).

In Vivo Evaluation Using Complete Freund Adjuvant–Induced Pain Model. We repeated the previous experiment with a longer-duration neuropathic pain model, where the drugs were administered via gavage for three consecutive days before complete Freund adjuvant (CFA) injection. On the morning of the experiment (6 h before CFA injection), the last dose of drugs was administered. CFA was injected in the right paw, while the left paw remained uninjected as a control. The testing involved two-stimulus thermal hyperalgesia using Hargreaves Test and mechanical allodynia using Von Frey Test on days 1, 2, 3, and 5.

Demeclocycline, DC, and MCD significantly prolonged the paw withdrawal latency of the injected paw compared to the controls upon exposure to thermal stimulus. The same behavior was observed upon exposure to mechanical stimulus with the three tested formulas, where the drug(s) effect starts to diminish significantly by day 5 (Fig. 4*B*).

We isolated the brain, dorsal root ganglion (DRG), and spinal cord from mice treated with PBS, demeclocycline, DC, and MCD to extract protein lysates and monitor for the phosphorylation state of EphB1 and EphB2 receptors (pEphB1/2) by Western blot as a measurement of catalytic activity and autophosphorylation. We found that MCD-treated samples significantly inhibit the phosphorylation of EphB 1/2 (Fig. 4 *D–F*). In addition, we isolated and sectioned spinal cords from mice treated with PBS and MCD

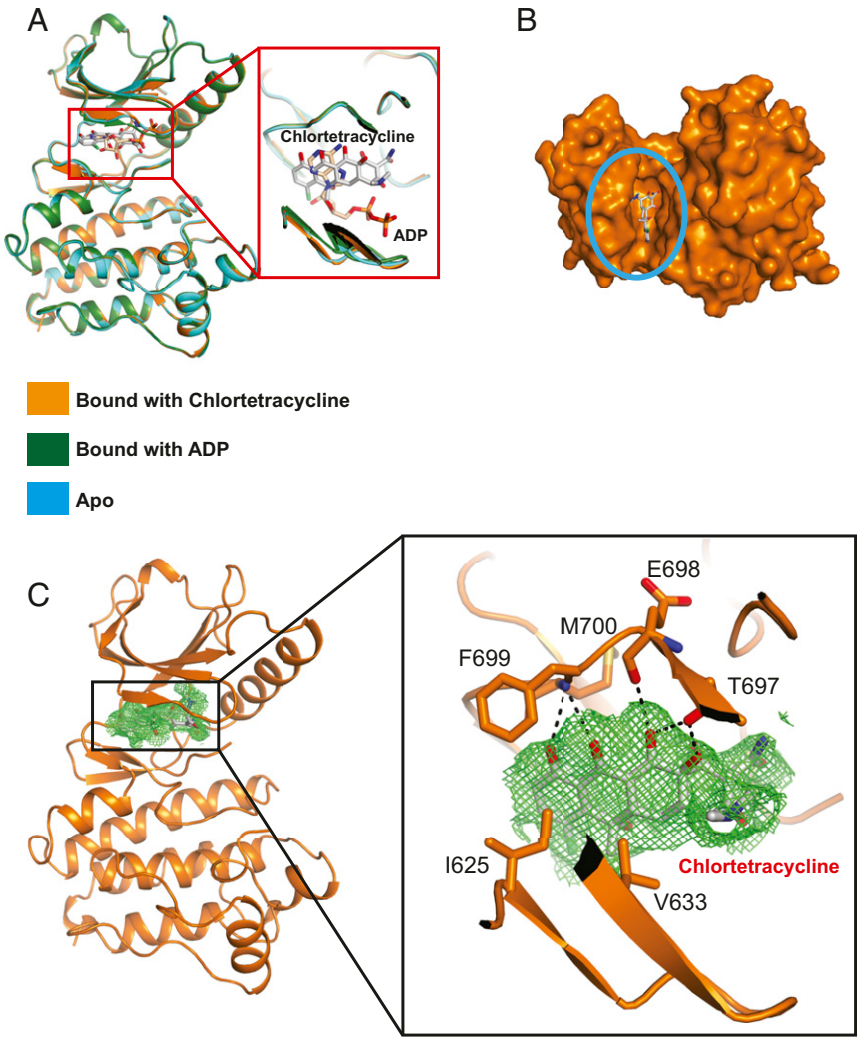

Fig. 3. Cocrystal structural analysis of EphB1 kinase domain bound with chlortetracycline. (*A*, *Left*) Ribbon representation showing superimposition of apo EphB1 (blue), EphB1 bound with ADP (green), and EphB1 bound with chlortetracycline (orange). (*A*, *Right*) Highlight of chlortetracycline and ADP in the ligand binding site. Chlortetracycline is shown in stick representation with backbone colored in gray, and ADP is shown in stick presentation with backbone colored in pink. (*B*) Space filling for chlortetracycline bound to the catalytic cavity of EphB1 kinase. (*C*, *Left*) Cartoon representation of the overall structure of EphB1 bound with chlortetracycline. EphB1 is shown in orange, and the polder map shows clear density (green mesh) for chlortetracycline, shown in stick representation with backbone colored in gray. (*C*, *Right*) Detailed interaction of chlortetracycline (gray sticks) in the ligand binding site. Specific residues making contacts with chlortetracycline are shown in orange sticks and labeled with black text. Hydrogen bonds are indicated with black dashed lines.

after fixing and immunostained with NeuN antibodies (neurons) and pEphB1/2 antibodies for the activated form of EphB receptors. We found that pEphB1/2 signal was reduced in the dorsal horn neurons in MCD-treated spinal cords compared to PBS-treated samples, confirming the inhibitory effect of MCD on phosphorylation of EphB 1/2 (Fig. 4*G*).

In Vivo Evaluation Using Formalin Test (a Model of Tissue Injury). In addition to the CFA and capsaicin models, we used formalin injection as a model for persistent pain following tissue injury. The tetracyclines were administered via gavage for three consecutive d before formalin injection. On the morning of the experiment, the last dose of drugs was administered. We recorded lifting/favoring and licking/biting responses of the injected paw by formalin for 60 min. Typically, the formalin response results in a biphasic pain response: Phase 1, which represents the acute nociception, lasts for 10 to 15 min and is followed by phase 2, which represents pain resumption and lasts for 30 to 40 min (53, 54).

During phase 1, we found no significant differences between PBS- and drug-treated mice. However, in phase 2, demeclocycline-, DC-, and MCD-treated mice showed significantly reduced lifting/favoring and licking/biting behavior compared to PBS-treated mice after formalin injection (Fig. 4*C*). In addition, we isolated spinal cords from mice treated with PBS and MCD and performed immunostaining for c-Fos as a marker of neuronal activation in response to formalin injection (after 60 min). We found that spinal cords from MCD-treated mice showed a significant reduction in the expression c-Fos compared to PBS-treated mice (Fig. 4*H*).

Discussion

Ephrin-Eph receptor mediated signaling has been implicated in numerous clinically relevant pathways. Ephrins and Eph receptors are expressed in almost all tissues in the mammalian embryo where they regulate a wide range of developmental pathways ranging from neuronal development and axonal guidance to cardiovascular development. In addition to their critical roles in development, Eph/ephrin are increasingly recognized as important modulators of various disease processes including neurological diseases and malignancy. Not surprisingly, there has been increasing interest in targeting ephrins and Eph receptors pharmacologically in

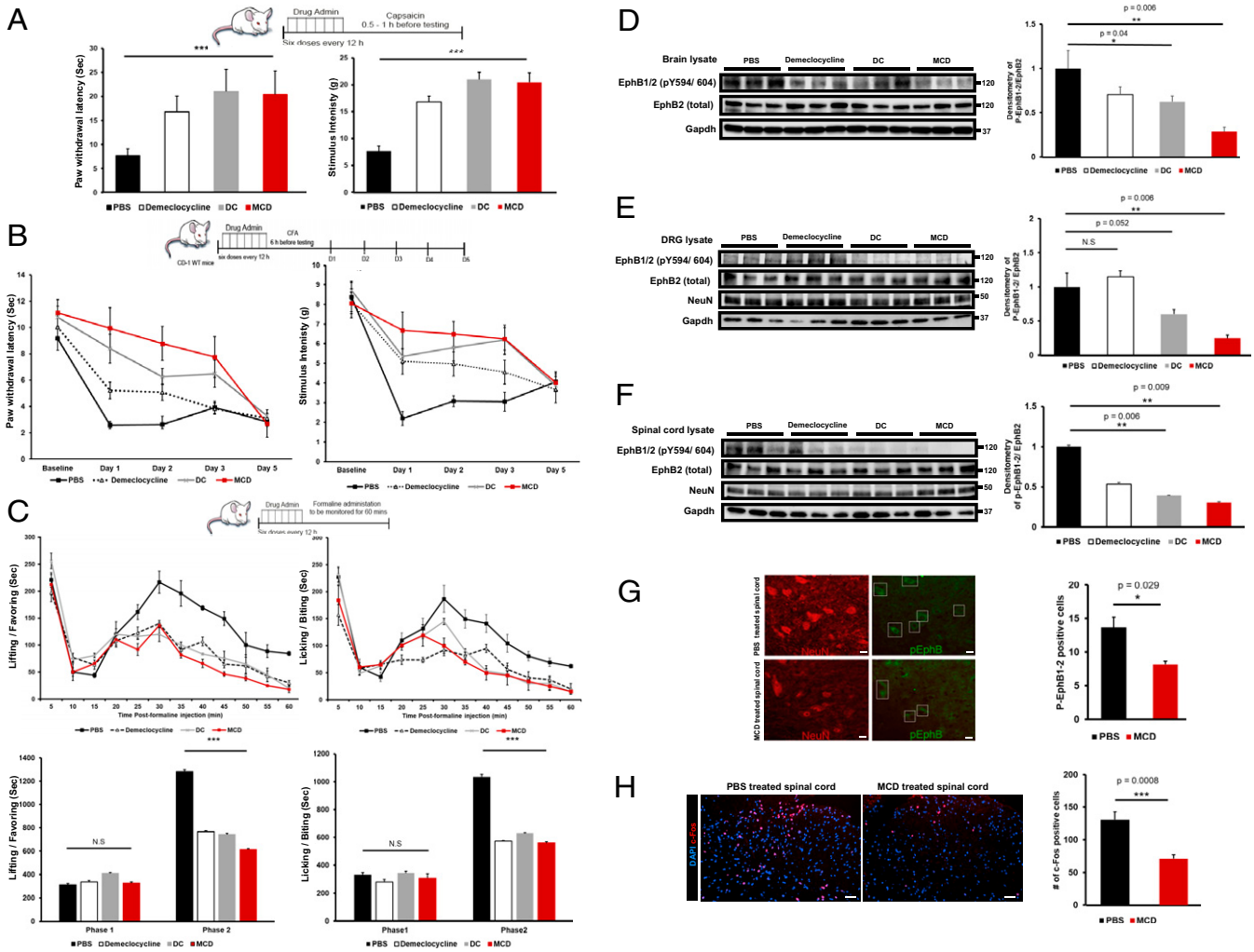

Fig. 4. In vivo biological evaluation of the drugs for thermal hyperalgesia and mechanical allodynia reversal effect. (*A*) Capsaicin-induced pain model; the development of thermal hyperalgesia using Hargreaves and mechanical allodynia using von Frey filaments after intraplantar right hind paw injection of 0.01% capsaicin for PBS-, demeclocycline-, DC-, and MCD-treated mice. The left hind paw remained uninjected. Demeclocycline, DC, and MCD prolong the paw withdrawal latency of the injected paw significantly compared to the PBS-treated mice at $***P < 0.001$; significant difference is based on the PBS (control) group. One-way ANOVA was conducted; data are expressed as mean ± SE ($n = 5$). (*B*) CFA-induced pain model; the development of thermal hyperalgesia using Hargreaves and mechanical allodynia using von Frey after intraplantar right paw injection of CFA for PBS-, demeclocycline-, DC-, and MCD-treated mice. The left paw was uninjected. A repeated-measures ANOVA followed by post hoc tests using the Bonferroni correction was conducted. Data are expressed as mean ± SE ($n = 5$). Demeclocycline showed significant improvement in the paw withdrawal latency for thermal hyperalgesia stimulus between time points until day 2 (F [2.451, 34.317] = 55.960, $***P < 0.001$); however, it only showed significant improvement to reverse the tactile allodynia stimuli at day 1 (F [3.441, 44.737] = 28.999, $***P < 0.001$), suggesting that the demeclocycline effect was significantly diminished by day 2. DC showed significant improvement in the paw withdrawal latency for thermal hyperalgesia and mechanical allodynia stimuli between time points until day 3 (F [2.072, 29.012] = 31.885, $***P < 0.001$) and (F [2.125, 19.122] = 24.320, $***P < 0.001$), respectively, suggesting that the DC effect was significantly diminished by day 5. MCD showed significant improvement in the paw withdrawal latency for thermal hyperalgesia and mechanical allodynia stimuli between time points until day 3 (F [2.015, 28.215] = 16.419, $***P < 0.001$) and (F [2.471, 24.711] = 14.525, $***P < 0.001$), respectively; suggesting that MCD effect was significantly diminished by day 5. (*C*) Formalin-induced pain model; the development of biphasic behavioral responses (lifting/favoring and licking/biting) after intraplantar right paw injection of 5% formalin for PBS-, demeclocycline-, DC-, and MCD-treated mice. During phase 1, there was no significant difference between PBS- and drug-treated mice; however, in phase 2, demeclocycline-, DC-, and MCD-treated mice significantly reduced the lifting/favoring and licking/biting behaviors compared to PBS-treated mice after formalin injection at $***P < 0.001$; significant difference is based on the PBS (control) group. One-way ANOVA was conducted; data are expressed as mean ± SE ($n = 5$). (*D*) Western blotting and densitometry analysis for PBS-, demeclocycline-, DC-, and MCD-treated brain lysates, showing that MCD significantly inhibits the phosphorylation of EphB 1/2 at $**P < 0.01$; significant difference is based on the PBS (control) group. Student's *t* test was conducted; data are expressed as mean ± SE ($n = 3$). (*E*) Western blotting and densitometry analysis for PBS-, demeclocycline-, DC-, and MCD-treated DRG lysates, showing that MCD significantly inhibits the phosphorylation of EphB 1/2 at $**P < 0.01$; significant difference is based on the PBS (control) group. Student's *t* test was conducted; data are expressed as mean ± SE ($n = 3$). (*F*) Western blotting and densitometry analysis for PBS-, demeclocycline-, DC-, and MCD-treated spinal cord lysates, showing that MCD significantly inhibits the phosphorylation of EphB 1/2 at $**P < 0.01$; significant difference is based on the PBS (control) group. Student's *t* test was conducted; data are expressed as mean ± SE ($n = 3$). (*G*) Immunostaining and quantification for PBS-treated versus MCD-treated spinal cords, showing that phosphorylated form of EphB1/2 receptors was diminished significantly in the MCD-treated spinal cord to suggest the ability of MCD to inhibit the phosphorylation of EphB1/2 at $*P < 0.05$; significant difference is based on the PBS (control) group. Student's *t* test was conducted; data are expressed as mean ± SE ($n = 3$). Neurons were stained with NeuN (red) and pEphB2 (green) antibodies. (*H*) Immunostaining and quantification for PBS-treated versus MCD-treated spinal cords after formalin injection, showing that c-Fos expression was significantly reduced in the MCD-treated spinal cord at $***P < 0.001$; significant difference is based on the PBS (control) group. Student's *t* test was conducted; data are expressed as mean ± SE ($n = 3$). C-fos was stained in red and nuclei was stained in blue DAPI antibodies.

recent years. For example, the Eph–ephrin interaction was recently targeted for drug discovery using high-throughput approaches to identify peptides and small-molecular-weight chemicals (55). These compounds dock into a deep pocket formed in the N-terminal globular ephrin-binding domain of the Eph receptor ectodomain within the G-H loop and disrupt protein–protein interfaces involved in receptor-ligand dimerization (56). The intracellular Eph tyrosine kinase domain is the site where phosphorylation on Y594/604 occurs in the juxtamembrane domain, which is critical for the receptor activation (45, 57, 58).

Recently, a number of studies have demonstrated that targeting EphB receptor kinase domains is feasible. For example, in a recent elegant study, Kung et al. described an irreversible and specific inhibitor of the EphB3 kinase domain that covalently binds to the Cys717 residue, which is not present in the other Eph receptors (59), including EphB1 and EphB2 receptors outlined in the current study.

The tetracycline family is a class of bacteriostatic antibiotics which has been in clinical use since the 1970s. Of relevance to this publication, several tetracyclines have been known to have biological functions beyond their bacteriostatic activity. For example, demeclocycline use is well documented in noninfectious diseases where, before the development of vasopressin 2 blockers, demeclocycline was the cornerstone in the treatment of syndrome of inappropriate antidiuretic hormone (SIADH). This is a syndrome characterized by hyponatremia due to excessive antidiuretic hormone secretion, associated with supernormal reabsorption of free water from the collecting ducts. The reabsorption of water occurs through aquaporin channels in the collecting duct. While there is no known mechanism that can explain the effectiveness of demeclocycline in treatment of SIADH, it is intriguing to ponder whether this effect is related to its inhibitory effect on Eph receptors, especially that Ephs are known to bind to aquaporin water channels (60).

In the current report, we utilized a drug-repositioning strategy by applying conventional concepts of molecular similarity assessment followed by structure-based in silico screening to identify drug(s) with a well-documented therapeutic index and safety profiles to target the catalytic domain of EphB kinases. We determined the potential of chlortetracycline, demeclocycline, and minocycline to bind the catalytic domain of EphB kinases in terms of the following: 1) Tanimoto Coefficient index, 2) binding affinity based on the energy profile (ΔG), and 3) binding mode within the catalytic domain of the receptor of interest. We conducted further validation via in vitro kinase assays for inhibition of kinase activity of EphB receptors (EphB1-B4) for chlortetracycline, demeclocycline, and minocycline. The results from these kinase assays encouraged us to pursue dual- and triple-antibiotic combinations to test for their inhibitory potential against the kinase domain of EphB1-4. These drug combinations demonstrated a markedly improved IC_{50} compared to single drugs, an effect which can improve the therapeutic safety profile by using submaximal doses of each of the tetracyclines.

An important aspect of our current study is the structural biology aspect. First, although the structure of the EphB1 receptor has been known for some time, the receptor has not been previously crystallized with its ligand ATP/ADP. Therefore, we performed these studies, and we present a crystal structure of EphB1 receptor bound to ADP. Next, we cocrystalized chlortetracycline with EphB1 kinase domain to validate our hypothesis for the binding of the tetracycline family to the predicted target. Our crystal structure outlines the structure basis for the interaction of the three tetracyclines with EphB1. Importantly, the crystal structures demonstrate that these tetracyclines interact with critical amino acid residues in the substrate binding pocket that are required for ATP binding.

Based on these findings, we proceeded with in vivo biological evaluation to test the pharmacological profile for demeclocycline, DC, and MCD in three different neuropathic pain models including capsaicin, CFA, and formalin injection models. We found that demeclocycline, DC, and MCD effectively reverse thermal hyperalgesia and mechanical allodynia in both shorter duration (Capsaicin) and longer duration (CFA) models and completely blocked pain behavior which result from tissue damage in the formalin model. It is important to note that although minocycline has been previously reported to inhibit neuropathic pain in a number of elegant studies, which was attributed to modulation of microglia activation, the doses used in these studies yield a plasma concentration of less than 5 μM (61, 62), which is significantly below the IC_{50} for minocycline on EphB1 receptor (56 μM). Thus, we believe that the previously tested doses of minocycline that modulated microglia would not have impacted EphB1 kinase activity as a mechanism of neuropathic pain.

Conclusion

In summary, our results identify chlortetracycline, demeclocycline, and minocycline as inhibitors of EphB1 receptor activity by binding to the kinase domain (*SI Appendix*, Fig. S7). These results can be readily applicable clinically for treatment of neuropathic pain and potentially for other clinical scenarios where the underlying mechanism is dependent on EphB1/2 activation. Our results also provide proof of concept for the development of molecules for targeting Eph/ephrin-mediated pathologies.

Materials and Methods

Virtual Screening Strategy.

FDA-approved small molecules preparation. The US FDA–approved drug database was downloaded (https://go.drugbank.com/), and three-dimensional structures were energy minimized using MMFF94 force field (63).

X-ray crystal structure preparation. Crystal structure of the EphB1 catalytic domain has been resolved in the Protein data bank (PDB codes: 3ZFX and 5MJA), Staurosporine, EphB4 kinase inhibitor (PDB code: 3EZW), was used as a query for ligand-based drug design due to the scaffold complexity that could offer potential diverse scaffolds.

Ligand-based in silico screening. The energy minimized two-dimensional (2D) structure comparison between staurosporine and the FDA-approved small molecules library was performed by Molecular Operating Environment (MOE) to assign the degree of structural similarity. The top scoring compounds were selected based on Tanimoto coefficient score ranging from 1 to 0.5 to undergo docking (*SI Appendix*, Table S1).

Structure-based in silico screening and scoring. The top ten selected energy minimized approved small molecules, based on literature survey and clinical indications underwent docking simulations using MOE along with EphB1 kinase domain (PDB ID; 5MJA). The top selected energy minimized compounds underwent protonation state to add the missing hydrogens for proper ionization states (64, 65). MOE Dock application was used to find the favorable binding conformations/poses for the studied candidates. The scoring assessment was conducted by validating the docked poses using the London dG scoring method to estimate the energy profile showing the potential hydrophobic and hydrogen bond interactions. Three-dimensional visualization was generated using Chimera (66), while the 2D generation was done using MOE tools (*SI Appendix*, Fig. S1).

Biochemical Evaluation.

IC_{50} profiling for EphB1 kinase activity. Seven FDA-approved drugs were selected to enroll a radiometric protein kinase assay (^{33}P PanQinase Activity Assay, ProQinase) to measure the effect of increasing concentrations of compound on catalytic activity of the EphB1, EphB2, EphB3, and EphB4 kinase domains. ProQinase using human complimentary DNAs (cDNAs) to express recombinant GST/His's–fusion proteins purified by affinity chromatography and determined to be enzymatically active by phosphorylation of a Poly (Glu, Tyr) substrate produced kinase domain. The FDA compounds were assayed in 10 concentrations in the range from 1×10^{-4} M to 3×10^{-9} M for their ability to effect kinase activities. The final dimethyl sulfoxide (DMSO) concentration in the reaction mixtures was 1% in all cases. Kinase assays were performed in 96-well FlashPlates from PerkinElmer in a 50-μL reaction volume. The reaction mixture was pipetted in four steps in the following order: 20 μL assay buffer (standard buffer), 5 μL ATP solution (in H_2O), 5 μL test compound (in 10% DMSO), and 20 μL enzyme/substrate mix. The assay for the protein kinase contained 70 mM Hepes–NaOH, pH 7.5, 3 mM $MgCl_2$,

3 mM $MnCl_2$, 3 μM Na-orthovanadate, 1.2 mM dithiothreitol (DTT), 50 μg/mL PEG20000, ATP (corresponding to the apparent ATP-K_m of the kinase), [γ-^{33}P]-ATP [approximately 2×10^5 counts per million (cpm) per well], protein kinase, and substrate. The reaction mixtures were incubated at 30 °C for 60 min. The reaction was stopped with 50 μL 2% (vol/vol) H_3PO_4, plates were aspirated and washed two times with 200 μL 0.9% (wt/vol) NaCl. Incorporation of ^{33}Pi was determined with a microplate scintillation counter (Microbeta, Wallac). All assays were performed with a BeckmanCoulter/SAGIAN Core System. The median value of the counts in column 1 ($n = 8$) of each assay plate was defined as "low control." This value reflects unspecific binding of radioactivity to the plate in the absence of a protein kinase but in the presence of the substrate. The median value of the counts in column 7 of each assay plate ($n = 8$) was taken as the "high control" (i.e., full activity in the absence of any inhibitor). The difference between high and low control was taken as 100% activity. As part of the data evaluation, the low control value from a particular plate was subtracted from the high control value as well as from all 80 "compound values" of the corresponding plate. The residual activity (in %) for each well of a particular plate was calculated using the following formula:

$$\text{Res. Activity (\%)} = 100 \times [(\text{cpm of compound} - \text{low control}) / (\text{high control} - \text{low control})].$$

The residual activities for each concentration and the compound IC_{50} values were calculated using Quattro Workflow version 3.1.1 (Quattro Research GmbH; www.quattro-research.com/). The fitting model for the IC_{50} determinations was "Sigmoidal response (variable slope)" with parameters "top" fixed at 100% and "bottom" at 0%. The fitting method used was least squares fit.

Differential IC_{50} profiling for EphB protein kinase family. Chloride salts of demeclocycline, chlortetracycline, minocycline, DC, DM, MC, and MCD were selected to be screened against EphB1, EphB2, EphB3, and EphB4 and using 33PanQinase Activity Assay, as previously described. For each kinase, the median value of the cpm of three wells with complete reaction mixtures, but without kinase, was defined as "low control." This value reflects unspecific binding of radioactivity to the plate in the absence of protein kinase but in the presence of the substrate. Additionally, for each kinase the median value of the cpm of three other wells with the complete reaction mixture, but without any compound, was taken as the "high control" (i.e., full activity in the absence of any inhibitor [$n = 3$]). The difference between high and low control was taken as 100% activity for each kinase. As part of the data evaluation, the low control of each row of a particular plate was subtracted from the high control value as well as from their corresponding "compound values." The residual activity (in percent) for each well of each row of a particular plate was calculated by using the following formula:

$$\text{Res. Activity (\%)} = 100 \times [(\text{cpm of compound} - \text{low control}) / (\text{high control} - \text{low control})].$$

Since 10 distinct concentrations of each test compound were tested against each kinase, the evaluation of the raw data resulted in 10 values for residual activities per kinase. Based on each 10 corresponding residual activities, IC_{50} values were calculated using Prism 5.04 for Windows (Graphpad; https://www.graphpad.com/). The mathematical model used was "Sigmoidal response (variable slope)" with parameters "top" fixed at 100% and "bottom" at 0%.

Selectivity profiling of 40 μM MCD against 88 protein tyrosine and tyrosine-like kinases. A radiometric protein kinase assay (^{33}PanQinase Activity Assay) was used for measuring the kinase activity of tyrosine and tyrosine-like kinases. All kinase assays were performed in 96-well FlashPlates from Perkin-Elmer in a 50-μL reaction volume. The reaction mixture was prepared in the following order via addition of the following: 1) 10 μL nonradioactive ATP solution (in H_2O), 2) 25 μL assay buffer/[γ- ^{33}P]-ATP mixture, 3) 5 μL test sample in 10% DMSO, and 4) 10 μL enzyme/substrate mixture. The assay for all protein kinases contained 70 mM Hepes-NaOH pH = 7.5, 3 mM $MgCl_2$, 3 mM $MnCl_2$, 3 μM Na-orthovanadate, 1.2 mM DTT, 50 μg/mL PEG20000, ATP (variable amounts, corresponding to the apparent ATP-K_m of the respective kinase), [γ- ^{33}P]-ATP (approximately $8 \times 1{,}005$ cpm per well), protein kinase, and substrate.

$$\text{Res. Activity (\%)} = 100 \times [(\text{signal of compound} - \text{low control}) / (\text{high control} - \text{low control})]$$

Protein Expression and Purification. h*Ephb1* with residues 602 to 896 was subcloned into pETDuet vector with noncleavable N-terminal 6xHis tag and transformed into Rosetta (DE3) pLysS cells (Novagen). Target protein was expressed in cultures grown in autoinduction media at 18 °C overnight (67). The culture was harvested and sonicated in lysis buffer (50 mM Tris [pH = 8.0], 1 M NaCl, 1 mM DTT, and supplemented with protease inhibitors). The lysate was centrifuged, the supernatant was loaded onto a Ni-NTA affinity column (Qiagen), and the beads were washed with wash buffer (20 mM Tris [pH = 8.0], 1 M NaCl, 1 mM DTT, and 20 mM Imidazole [pH = 8.0]) and eluted with elution buffer (20 mM Tris [pH = 8.0], 150 mM NaCl, 1 mM DTT, and 250 mM Imidazole [pH = 8.0]). The eluate was concentrated and purified by gel filtration chromatography. The peak fractions were collected and concentrated to about 10 mg/mL for crystallization screening.

Crystallization and structure determination. The crystals of the apo h*Ephb1* were obtained using the hanging-drop, vapor-diffusion method by mixing 1 μL protein (10 mg/mL) with 1 μL reservoir solution containing 0.2 M Sodium Malonate (pH = 4.6) and 14% PEG 3350 and incubating at 18 °C. The crystals were observed after 2 d and reached the maximum size after 5 d. The complex crystals with chlortetracycline were generated by soaking the apo crystals with 30-mM compound for 6 h at 18 °C. The complex crystals with ADP were generated by incubating ADP with the protein at 1:6 ratio at room temperature for 1 h, mixing with the reservoir solution, and then incubating at 18 °C. The datasets were collected at APS-19-ID at wavelengths of 0.97926 and 0.97918 Å, respectively. Data were indexed, integrated, and scaled by the program HKL3000 (68). Phases were determined by molecular replacement using the apo Ephb1 structure (PDB code: 3ZFX) as a searching model. The model was further built manually with Crystallographic Object-Oriented Toolkit (COOT) (69) and iteratively refined using Phenix.refine (70). The PROCHECK program was used to check the quality of the final model, which shows good stereochemistry according to the Ramachandran plot (71). All structure figures were generated by using the PyMOL Molecular Graphics System, Schrödinger, LLC. Software used in this project was curated by SBGrid (72).

In Vivo Biological Evaluation.

Animals. A total of 40 male outbred CD1 mice were obtained from Charles River Laboratories at 8 wk of age. Mice were housed in the animal facility of UT southwestern Medical Center, with constant temperature (21 to 24 °C) and humidity (30 to 50%) with free access to standard animal feed and water. The room was kept on a 12/12 light/dark cycle, with white light (light cycle) on at 2,400 h and red lights (dark cycle) on at 1,200 h. All of the procedures were conducted with approval from the University of Texas (UT) Southwestern Medical Center Institutional Animal Care and Use Committee (IACUC Protocol No. 2017-102090). Ugo Basile, the original Plantar Test (Hargreaves Apparatus), was used for thermal stimulation, where infrared beam was adjusted to give an average paw withdrawal latency of about 10 s in wild-type (WT) mice, and cutoff time was set to 30 s to avoid tissue damage. Ugo Basile Dynamic Plantar Aesthesiometer for mechanical stimulation (Electronic Von Frey) were used for mechanical stimulation, where the force (grams) was set at 50 g to prevent tissue damage. Animals were placed in clear acrylic cubicles ($22 \times 16.5 \times 14$ cm) for at least 1 h prior to testing. The testing/recording was done every 5 min with no repetition for the same mouse. Blinded person(s) to the individual treatment assignments recorded true reflexes.

Drugs. Demeclocycline, minocycline, and chlortetracycline were freely soluble in PBS at their dose levels, purchased from Sigma Aldrich. DC was prepared by having an equimolar ratio of demeclocycline and chlortetracycline dissolved in PBS; 100 μL of the whole solution was administered per mouse via oral gavage. MCD was prepared by having an equimolar ratio of demeclocycline, minocycline, and chlortetracycline dissolved in PBS; 100 μL of the whole solution was administered per mouse via oral gavage. Capsaicin was dissolved in 5% Tween 80 and 5% ethanol and brought to volume with PBS; 5 μL was injected in the right paw of the mice. Complete freund's adjuvant contained 1 mg *Mycobacterium tuberculosis* (H37Ra, American Type Culture Collection 25177) per milliliter of emulsion in 85% paraffin oil and 15% mannide monooleate, and 5 μL was injected in the right paw of the mice.

Capsaicin pain model. Four different groups of CD-1 WT mice ($n = 5$, each) were assigned to represent four different treatments including control (PBS), demeclocycline (20 mg/kg/day/p.o), DC (7 mg/kg/day/p.o), and MCD (5 mg/kg/day/p.o). The drugs' dosage regimen was split to be administered every 12 h. Drugs were administered via gavage for seven doses interval before capsaicin injection.

Capsaicin (dissolved in 5% Tween 80 and 5% ethanol and brought to volume with PBS) was injected in the right hind paw, while the left hind paw remained uninjected as control. The testing involved two stimulus thermal hyperalgesia using Hargreaves Test and mechanical allodynia using Von Frey Test. The whole experiment was conducted within 1 to 2 h.

CFA pain model. Four different groups of CD-1 WT mice (n = 5 each) were assigned to represent four different treatments, including control (PBS), demeclocycline (20 mg/kg/day/p.o), DC (7 mg/kg/day/p.o), and MCD (5 mg/kg/day/p.o). The drugs' dosage regimen was split to be administered every 12 h. Drugs were administered via gavage for seven doses interval before capsaicin injection. A baseline was detected for the mice behavior toward thermal hyperalgesia using Hargreaves Test and mechanical allodynia using Von Frey Test prior to drug(s) administration. The drugs were administered via gavage for three consecutive days before CFA contained 1 mg of *M. tuberculosis* (H37Ra, American Type Culture Collection 25177) per milliliter of emulsion in 85% paraffin oil and 15% mannide monooleate) injection. On the morning of the experiment (6 h before CFA injection), the last dose of drugs was administered. CFA was injected in the right hind paw, while the left hind paw remained uninjected as control. The testing involved two-stimulus thermal hyperalgesia using Hargreaves Test and mechanical allodynia using Von Frey Test at Days 1, 2, 3, and 5.

Formalin pain model. Four different groups of CD-1 WT mice (n= 5, each) were assigned to represent four different treatment groups including control (PBS), demeclocycline (20 mg/kg/day/p.o), DC (7 mg/kg/day/p.o), and MCD (5 mg/kg/day/p.o). The drugs' dosage regimen was split to be administered every 12 h. Drugs were administered via gavage for seven doses interval before Formalin injection. The formalin was prepared by injecting 5% formaldehyde solution into the plantar surface of the right hind paw, while the left paw remained uninjected as control. The testing involved monitoring lifting/favoring and biting/licking pain responses for 60 min.

Lysates preparation and Western blotting. Brains, spinal cords, and DRG were isolated and lysed in radioimmunoprecipitation assay (RIPA) buffer with the addition of Complete protease inhibitor mixture (Roche). Protein concentration was quantified using Pierce BCA protein assay kit (Pierce Biotechnology) with three biological replicates. After separation via sodium dodecyl sulphate–polyacrylamide gel electrophoresis (SDS-PAGE), proteins were transferred to nitrocellulose membranes (Bio-Rad), blocked in 5% skim milk/TBS, and incubated with appropriate primary antibodies as follows: anti-Eph receptor B1 + Eph receptor B2 (phospho Y594 + Y604) antibody (Abcam, ab61791, 1:200), anti-Human/Mouse EphB2 Antibody (R&D system, AF467, 1:1,000), and anti-Gapdh (Sigma, AB2302, 1:5,000). Horseradish peroxidase–conjugated peroxidase anti-rabbit, anti-chicken, or anti-goat antibodies (1:25,000 to 1:50,000) were used as secondary antibodies. The membranes were explored using Licor Odyssey Fc system and quantified by Image Studio software.

Spinal cord isolation. The spinal cords were isolated from the spinal column by hydraulic extrusion method (73). The spinal cords were fixed in 4% paraformaldehyde for 2 h at 4 °C. After washing with PBS, the spinal cords were placed in 30% sucrose overnight at 4 °C and embedded in optimal cutting temperature (OCT) compound for Cryo section, with three biological replicates.

Immunostaining. Prior to the immunostaining, cryo-spinal cord sections were post fixed in 4% paraformaldehyde in 1× PBS for 10 min at room temperature and washed three times with 1× PBS. For antigen retrieval, the sections were steamed in epitope retrieval solution (IHC World) for 20 min and cooled down for 30 min at room temperature. Antigen retrieval was not applied for c-Fos staining. After washing with 1× PBS, the sections were permeabilized and blocked in 10% normal goat serum with 0.3% Triton X-100 for 30 min at room temperature. Then, sections were incubated with primary antibodies overnight at 4 °C. The sections were subsequently washed three times with 1× PBS and incubated with corresponding secondary antibodies conjugated to Alexa Fluor 488 or 555 (Invitrogen) at 1:400 ratio. Cell nuclei were counterstained with DAPI for 5 min. The sections were mounted in anti-fade mounting medium (Vector Laboratories). Primary antibodies used are as follows: anti-NeuN (Abcam, ab104224, 1:100), anti-pEphB 1/2 (Abcam, ab61791, 1:100; Eph receptor B1+Eph receptor B2 [Y594+Y604]), and antibody rabbit anti-c-Fos (1:2,000) (Invitrogen). Images were obtained using Nikon Eclipse Ni microscopes.

Data Availability. All study data are included in the article and/or *SI Appendix*.

ACKNOWLEDGMENTS. We thank Drs. Diana Tomchick and Zhe Chen for assistance with data collection. Results shown in this report are derived from work performed at Argonne National Laboratory, Structural Biology Center (SBC) at the Advanced Photon Source. SBC is operated by the US Department of Energy, Office of Biological and Environmental Research under Contract DE-AC02-06CH11357. M.H. acknowledges support from the Kent Waldrep Center for Basic Research on Nerve Growth and Regeneration.

1. B. A. Martell *et al*., Systematic review: Opioid treatment for chronic back pain: Prevalence, efficacy, and association with addiction. *Ann. Intern. Med.* **146**, 116–127 (2007).
2. A. Slomski, Cultural transformation needed to solve public health problem of chronic pain. *JAMA* **306**, 692–693 (2011).
3. P. M. Lippe, C. Brock, J. David, R. Crossno, S. Gitlow, The first national pain medicine summit–Final summary report. *Pain Med.* **11**, 1447–1468 (2010).
4. D. E. Joranson, A. M. Gilson, Drug crime is a source of abused pain medications in the United States. *J. Pain Symptom Manage.* **30**, 299–301 (2005).
5. A. M. Trescot, S. Datta, M. Lee, H. Hansen, Opioid pharmacology. *Pain Physician* **11**(suppl. 2), S133–S153 (2008).
6. E. Kandil, E. Melikman, B. Adinoff, Lidocaine infusion: A promising therapeutic approach for chronic pain. *J. Anesth. Clin. Res.* **8**, 697 (2017).
7. L. Colloca *et al*., Neuropathic pain. *Nat. Rev. Dis. Primers* **3**, 17002 (2017).
8. P. Marchettini, M. Lacerenza, E. Mauri, C. Marangoni, Painful peripheral neuropathies. *Curr. Neuropharmacol.* **4**, 175–181 (2006).
9. G. Andreisek, D. W. Crook, D. Burg, B. Marincek, D. Weishaupt, Peripheral neuropathies of the median, radial, and ulnar nerves: MR imaging features. *Radiographics* **26**, 1267–1287 (2006).
10. K. T. Brizzi, J. L. Lyons, Peripheral nervous system manifestations of infectious diseases. *Neurohospitalist* **4**, 230–240 (2014).
11. A. K. Schreiber, C. F. Nones, R. C. Reis, J. G. Chichorro, J. M. Cunha, Diabetic neuropathic pain: Physiopathology and treatment. *World J. Diabetes* **6**, 432–444 (2015).
12. C. S. Cleeland, J. T. Farrar, F. H. Hausheer, Assessment of cancer-related neuropathy and neuropathic pain. *Oncologist* **15** (suppl. 2), 13–18 (2010).
13. R. E. Ferner, R. A. Hughes, S. M. Hall, M. Upadhyaya, M. R. Johnson, Neurofibromatous neuropathy in neurofibromatosis 1 (NF1). *J. Med. Genet.* **41**, 837–841 (2004).
14. J. Rivera-Zayas, M. Arroyo, E. Mejias, Evaluation of Persian Gulf veterans with symptoms of peripheral neuropathy. *Mil. Med.* **166**, 449–451 (2001).
15. R. M. Thomson, G. J. Parry, Neuropathies associated with excessive exposure to lead. *Muscle Nerve* **33**, 732–741 (2006).
16. R. F. White *et al*., Recent research on Gulf War illness and other health problems in veterans of the 1991 Gulf War: Effects of toxicant exposures during deployment. *Cortex* **74**, 449–475 (2016).
17. D. Fornasari, Pharmacotherapy for neuropathic pain: A review. *Pain Ther.* **6** (suppl. 1), 25–33 (2017).
18. M. C. Rowbotham *et al*., Oral opioid therapy for chronic peripheral and central neuropathic pain. *N. Engl. J. Med.* **348**, 1223–1232 (2003).
19. V. Cibert-Goton *et al*., Involvement of EphB1 receptors signalling in models of inflammatory and neuropathic pain. *PLoS One* **8**, e53673 (2013).
20. E. B. Pasquale, Eph receptors and ephrins in cancer: Bidirectional signalling and beyond. *Nat. Rev. Cancer* **10**, 165–180 (2010).
21. Y. Han, X. S. Song, W. T. Liu, M. Henkemeyer, X. J. Song, Targeted mutation of EphB1 receptor prevents development of neuropathic hyperalgesia and physical dependence on morphine in mice. *Mol. Pain* **4**, 60 (2008).
22. W. T. O'Neal *et al*., Ephrin-Eph signaling as a potential therapeutic target for the treatment of myocardial infarction. *Med. Hypotheses* **80**, 738–744 (2013).
23. L. Y. Liang, O. Patel, P. W. Janes, J. M. Murphy, I. S. Lucet, Eph receptor signalling: From catalytic to non-catalytic functions. *Oncogene* **38**, 6567–6584 (2019).
24. T. W. Vanderah, M. H. Ossipov, J. Lai, T. P. Malan, Jr, F. Porreca, Mechanisms of opioid-induced pain and antinociceptive tolerance: Descending facilitation and spinal dynorphin. *Pain* **92**, 5–9 (2001).
25. C. G. Parsons, NMDA receptors as targets for drug action in neuropathic pain. *Eur. J. Pharmacol.* **429**, 71–78 (2001).
26. R. R. Ji, T. Kohno, K. A. Moore, C. J. Woolf, Central sensitization and LTP: Do pain and memory share similar mechanisms? *Trends Neurosci.* **26**, 696–705 (2003).
27. R. Drdla, M. Gassner, E. Gingl, J. Sandkühler, Induction of synaptic long-term potentiation after opioid withdrawal. *Science* **325**, 207–210 (2009).
28. J. Sandkühler, D. Gruber-Schoffnegger, Hyperalgesia by synaptic long-term potentiation (LTP): An update. *Curr. Opin. Pharmacol.* **12**, 18–27 (2012).
29. A. A. Battaglia, K. Sehayek, J. Grist, S. B. McMahon, I. Gavazzi, EphB receptors and ephrin-B ligands regulate spinal sensory connectivity and modulate pain processing. *Nat. Neurosci.* **6**, 339–340 (2003).
30. X. J. Song *et al*., Upregulation and redistribution of ephrinB and EphB receptor in dorsal root ganglion and spinal dorsal horn neurons after peripheral nerve injury and dorsal rhizotomy. *Eur. J. Pain* **12**, 1031–1039 (2008).
31. W. T. Liu, H. C. Li, X. S. Song, Z. J. Huang, X. J. Song, EphB receptor signaling in mouse spinal cord contributes to physical dependence on morphine. *FASEB J.* **23**, 90–98 (2009).
32. X. J. Song *et al*., EphrinB-EphB receptor signaling contributes to neuropathic pain by regulating neural excitability and spinal synaptic plasticity in rats. *Pain* **139**, 168–180 (2008).
33. J. L. Cao *et al*., Activation of peripheral ephrinBs/EphBs signaling induces hyperalgesia through a MAPKs-mediated mechanism in mice. *Pain* **139**, 617–631 (2008).
34. J. Zhao *et al*., Nociceptor-expressed ephrin-B2 regulates inflammatory and neuropathic pain. *Mol. Pain* **6**, 77 (2010).
35. W. S. Xia *et al*., Spinal ephrinB/EphB signalling contributed to remifentanil-induced hyperalgesia via NMDA receptor. *Eur. J. Pain* **18**, 1231–1239 (2014).
36. I. Vasileiou, I. Adamakis, E. Patsouris, S. Theocharis, Ephrins and pain. *Expert Opin. Ther. Targets* **17**, 879–887 (2013).
37. M. Henkemeyer, O. S. Itkis, M. Ngo, P. W. Hickmott, I. M. Ethell, Multiple EphB receptor tyrosine kinases shape dendritic spines in the hippocampus. *J. Cell Biol.* **163**, 1313–1326 (2003).

38. Y. Yamaguchi, E. B. Pasquale, Eph receptors in the adult brain. *Curr. Opin. Neurobiol.* **14**, 288–296 (2004).
39. R. Klein, Bidirectional modulation of synaptic functions by Eph/ephrin signaling. *Nat. Neurosci.* **12**, 15–20 (2009).
40. K. O. Lai, N. Y. Ip, Synapse development and plasticity: roles of ephrin/Eph receptor signaling. *Curr. Opin. Neurobiol.* **19**, 275–283 (2009).
41. M. J. Nolt *et al*., EphB controls NMDA receptor function and synaptic targeting in a subunit-specific manner. *J. Neurosci.* **31**, 5353–5364 (2011).
42. N. J. Xu, M. Henkemeyer, Ephrin reverse signaling in axon guidance and synaptogenesis. *Semin Cell Dev. Biol.* **23**, 58–64 (2012).
43. I Gavazzi, "EphB receptors and persistent pain" in *An Introduction to Pain and its Relation to Nervous System Disorders*, A. A. Battaglia, Ed. (John Wiley & Sons, 2016), pp. 201–224.
44. I. Chopra, P. M. Hawkey, M. Hinton, Tetracyclines, molecular and clinical aspects. *J. Antimicrob. Chemother.* **29**, 245–277 (1992).
45. K. L. Binns, P. P. Taylor, F. Sicheri, T. Pawson, S. J. Holland, Phosphorylation of tyrosine residues in the kinase domain and juxtamembrane region regulates the biological and catalytic activities of Eph receptors. *Mol. Cell. Biol.* **20**, 4791–4805 (2000).
46. L. E. Wybenga-Groot *et al*., Structural basis for autoinhibition of the Ephb2 receptor tyrosine kinase by the unphosphorylated juxtamembrane region. *Cell* **106**, 745–757 (2001).
47. R. C. Overman, J. E. Debreczeni, C. M. Truman, M. S. McAlister, T. K. Attwood, Completing the structural family portrait of the human EphB tyrosine kinase domains. *Protein Sci.* **23**, 627–638 (2014).
48. A. Kung *et al*., A chemical-genetic approach to generate selective covalent inhibitors of protein kinases. *ACS Chem. Biol.* **12**, 1499–1503 (2017).
49. Z. Cournia, B. Allen, W. Sherman, Relative binding free energy calculations in drug discovery: Recent advances and practical considerations. *J. Chem. Inf. Model.* **57**, 2911–2937 (2017).
50. D. Bajusz, A. Rácz, K. Héberger, Why is Tanimoto index an appropriate choice for fingerprint-based similarity calculations? *J. Cheminform.* **7**, 20 (2015).
51. E. L. Dimitrov, J. Kuo, K. Kohno, T. B. Usdin, Neuropathic and inflammatory pain are modulated by tuberoinfundibular peptide of 39 residues. *Proc. Natl. Acad. Sci. U.S.A.* **110**, 13156–13161 (2013).
52. N. S. Gregory *et al*., An overview of animal models of pain: Disease models and outcome measures. *J. Pain* **14**, 1255–1269 (2013).
53. T. C. O'Connor, S. E. Abram, Inhibition of nociception-induced spinal sensitization by anesthetic agents. *Anesthesiology* **82**, 259–266 (1995).
54. M. Shibata, T. Ohkubo, H. Takahashi, R. Inoki, Modified formalin test: Characteristic biphasic pain response. *Pain* **38**, 347–352 (1989).
55. S. J. Riedl, E. B. Pasquale, Targeting the Eph system with peptides and peptide conjugates. *Curr. Drug Targets* **16**, 1031–1047 (2015).
56. R. Noberini, I. Lamberto, E. B. Pasquale, Targeting Eph receptors with peptides and small molecules: Progress and challenges. *Semin. Cell Dev. Biol.* **23**, 51–57 (2012).
57. E. Berrou *et al*., A mutation of the human *EPHB2* gene leads to a major platelet functional defect. *Blood* **132**, 2067–2077 (2018).
58. K. Hanamura *et al*., Extracellular phosphorylation of a receptor tyrosine kinase controls synaptic localization of NMDA receptors and regulates pathological pain. *PLoS Biol.* **15**, e2002457 (2017).
59. A. Kung *et al*., Development of specific, irreversible inhibitors for a receptor tyrosine kinase EphB3. *J. Am. Chem. Soc.* **138**, 10554–10560 (2016).
60. C. A. Cowan *et al*., EphB2 guides axons at the midline and is necessary for normal vestibular function. *Neuron* **26**, 417–430 (2000).
61. P. Vanelderen *et al*., Effect of minocycline on lumbar radicular neuropathic pain: A randomized, placebo-controlled, double-blind clinical trial with amitriptyline as a comparator. *Anesthesiology* **122**, 399–406 (2015).
62. K. Kobayashi *et al*., Minocycline selectively inhibits M1 polarization of microglia. *Cell Death Dis.* **4**, e525 (2013).
63. T. A. Halgren, Merck molecular force field. I. Basis, form, scope, parameterization, and performance of MMFF94. *J. Comput. Chem.* **17**, 490–519 (1996).
64. M. Naïm *et al*., Solvated interaction energy (SIE) for scoring protein-ligand binding affinities. 1. Exploring the parameter space. *J. Chem. Inf. Model.* **47**, 122–133 (2007).
65. P. Labute, Protonate3D: Assignment of ionization states and hydrogen coordinates to macromolecular structures. *Proteins* **75**, 187–205 (2009).
66. E. F. Pettersen *et al*., UCSF Chimera–A visualization system for exploratory research and analysis. *J. Comput. Chem.* **25**, 1605–1612 (2004).
67. F. W. Studier, Protein production by auto-induction in high density shaking cultures. *Protein Expr. Purif.* **41**, 207–234 (2005).
68. W. Minor, M. Cymborowski, Z. Otwinowski, M. Chruszcz, HKL-3000: The integration of data reduction and structure solution–From diffraction images to an initial model in minutes. *Acta Crystallogr. D Biol. Crystallogr.* **62**, 859–866 (2006).
69. P. Emsley, K. Cowtan, Coot: Model-building tools for molecular graphics. *Acta Crystallogr. D Biol. Crystallogr.* **60**, 2126–2132 (2004).
70. P. D. Adams *et al*., PHENIX: A comprehensive python-based system for macromolecular structure solution. *Acta Crystallogr. D Biol. Crystallogr.* **66**, 213–221 (2010).
71. R. A. Laskowski, M. W. MacArthur, D. S. Moss, J. M. Thornton, PROCHECK: A program to check the stereochemical quality of protein structures. *J. Appl. Cryst.* **26**, 283–291 (1993).
72. A. Morin *et al*., Collaboration gets the most out of software. *eLife* **2**, e01456 (2013).
73. M. Richner, S. B. Jager, P. Siupka, C. B. Vaegter, Hydraulic extrusion of the spinal cord and isolation of dorsal root ganglia in rodents. *J. Vis. Exp.* 55226 (2017).